Scaling Hot-Electron Generation to High-Power, Kilojoule-Class Laser-Solid Interactions

P. M. Nilson,[1,2] A. A. Solodov,[1,2] J. F. Myatt,[2] W. Theobald,[2] P. A. Jaanimagi,[2] L. Gao,[2] C. Stoeckl,[2] R. S. Craxton,[2] J. A. Delettrez,[2] B. Yaakobi,[2] J. D. Zuegel,[2] B. E. Kruschwitz,[2] C. Dorrer,[2] J. H. Kelly,[2] K. U. Akli,[3] P. K. Patel,[4] A. J. Mackinnon,[4] R. Betti,[1,2,5] T. C. Sangster,[2] and D. D. Meyerhofer[1,2,5]

[1]*Fusion Science Center for Extreme States of Matter and Fast Ignition Physics, University of Rochester, Rochester, New York, USA*
[2]*Laboratory for Laser Energetics, University of Rochester, Rochester, New York, USA*
[3]*General Atomics, San Diego, California, USA*
[4]*Lawrence Livermore National Laboratory, Livermore, California, USA*
[5]*Departments of Mechanical Engineering and Physics, University of Rochester, Rochester, New York, USA*
(Received 10 August 2009; revised manuscript received 8 September 2010; published 1 December 2010)

Thin-foil targets were irradiated with high-power ($1 \leq P_L \leq 210$ TW), 10-ps pulses focused to intensities of $I > 10^{18}$ W/cm^2 and studied with K-photon spectroscopy. Comparing the energy emitted in K photons to target-heating calculations shows a laser-energy-coupling efficiency to hot electrons of $\eta_{L\text{-}e} = 20 \pm 10\%$. Time-resolved x-ray emission measurements suggest that laser energy is coupled to hot electrons over the entire duration of the incident laser drive. Comparison of the K-photon emission data to previous data at similar laser intensities shows that $\eta_{L\text{-}e}$ is independent of laser-pulse duration from $1 \leq \tau_p \leq 10$ ps.

DOI: 10.1103/PhysRevLett.105.235001 PACS numbers: 52.50.Jm, 52.38.Kd, 52.70.La

High-intensity laser-solid interactions ($> 10^{18}$ W/cm^2) accelerate large numbers of thermal electrons to relativistic energies. These high-energy, MeV-scale electrons are a source of significant energy deposition within plasmas and are used extensively in plasma-based particle acceleration [1–3], warm dense matter creation [4], laboratory astrophysics [5], ultrafast γ-ray generation [6], and fast-ignition research [6,7]. Efficient hot-electron generation is of great importance for the energetic feasibility of these applications and has been studied intensively [6,8–16].

Previous solid-target experiments showed energy-conversion efficiencies into hot electrons ($\eta_{L\text{-}e}$) of up to several tens of percent for picosecond or shorter pulses of 1-μm light and laser intensities from $10^{18} \leq I \leq 10^{20}$ W/cm^2 [6,8–16]. With recent developments in laser technology, it is now possible to generate kilojoule-class, $\tau_p = 10$-ps pulses that can be focused to intensities of $I > 10^{18}$ W/cm^2 [17]. Such long-duration, high-intensity laser pulses hold great promise for high-energy applications that require rapid electron-energy deposition over time scales that are short compared to the typical hydrodynamic decompression times of solid and laser-compressed targets.

In fast ignition, laser-compressed deuterium and tritium are rapidly heated and ignited by a high-intensity laser pulse [6,7]. An intense, multikilojoule, 10- to 20-ps-long laser pulse is required to generate the ignition spark with optimal electron beam energies and currents for energy deposition within the fuel assembly. Knowledge of the coupling of a high-intensity laser into energetic electrons that heat the fuel, in addition to how this scales to ignition-class lasers, is critical for our understanding of spark generation and fast ignition.

Hot-electron generation in this regime, however, is only partially understood, particularly at high laser energies ($E_L > 1000$ J) and long laser-pulse durations ($\tau_p \sim 10$ ps), where no previous data exist because of the unavailability of suitably high-energy lasers. With increasing laser-pulse duration, a number of processes affect energy coupling to solid targets, including preplasma formation [18], electron transport [19], hole boring [20], and laser-driven shock formation [21]. Understanding these effects on energy coupling is crucial for scaling hot-electron generation to long-pulse, high-intensity lasers.

In this Letter, measurements are reported of the effect of laser-pulse duration on $\eta_{L\text{-}e}$. X-ray spectroscopic measurements of hot-electron generation in high-intensity laser-solid interactions show that the conversion efficiency is independent of laser-pulse duration. Thin-foil targets have been heated with hot electrons generated by $\tau_p = 10$-ps pulses focused to intensities of $I > 10^{18}$ W/cm^2, and $\eta_{L\text{-}e}$ has been inferred with K-photon spectroscopy. Comparing the energy emitted in K photons to target-heating calculations shows an energy-coupling efficiency to hot electrons of $\eta_{L\text{-}e} \sim 20\%$ with laser powers from $1 \leq P_L \leq 210$ TW. These are the first experiments to study hot-electron generation with intense $\tau_p = 10$-ps pulses at such high laser powers. Time-resolved x-ray emission measurements suggest that hot electrons are generated over the entire duration of the incident laser drive. The K-photon emission data are compared to other published data at similar laser intensities, showing for the first time that $\eta_{L\text{-}e}$ is independent of laser-pulse duration from $1 \leq \tau_p \leq 10$ ps.

The experiments were carried out using the Multi-Terawatt (MTW) [22,23] and the OMEGA EP [17] Laser

Facilities at the University of Rochester's Laboratory for Laser Energetics. For these experiments, the MTW laser delivered energies of up to $E_L = 10$ J in a $\tau_p = 10$-ps pulse at a wavelength of $\lambda_L = 1.054$ μm. The laser pulse was focused by an $f/3$, off-axis parabolic mirror at normal incidence to the target with an $R_{80} = 5$ μm, where R_{80} is the spot radius containing 80% of the laser energy, providing a laser intensity of $I = 1 \times 10^{18}$ W/cm^2. OMEGA EP delivered higher laser energies from $300 \leq E_L \leq 2100$ J in a $\tau_p = 10$-ps pulse at a wavelength of $\lambda_L = 1.054$ μm. An $f/2$, off-axis parabolic mirror focused the laser pulse at either 45° or normal incidence to the target with an $R_{80} = 25$ μm, providing laser intensities of up to $I \sim 10^{19}$ W/cm^2 (Fig. 1) [24]. The targets were Cu foils with dimensions that were varied between $600\times 600 \times 50$ μm^3 and $75 \times 75 \times 3$ μm^3, mounted on a 17-μm-thick silicon-carbide stalk.

Preplasma expansion prior to intense laser irradiation affects the energy coupling to solid targets and is caused by low laser contrast [18]. For these OMEGA EP shots, fast-diode measurements indicate that the laser pedestal typically reaches 6×10^{-7} of the peak laser power and contains 10^{-4} of the total laser-pulse energy [Fig. 1(b)]. Over this energy range, calculations made using the 1D radiation hydrodynamics code LILAC [25] indicate that the preplasma extends up to 5–10 μm between the critical- and the solid-density plasma.

The main diagnostic for measuring K-photon emission from the target was an absolutely calibrated, single-photon-counting x-ray spectrometer based on an SI-800 x-ray charge-coupled device [26]. A combination of heavy shielding and collimation, and a large target-to-spectrometer distance, reduces the number of Cu K-photon hits that are detected, satisfying the single-photon-counting regime, while reducing the hard x-ray flux. A graphite (HOPG) crystal spectrometer provided a complementary measurement of the K-photon yield [27]. The radiation emission time was measured using an ultrafast x-ray streak camera with a temporal resolution of about 2 ps [28].

Typical K-photon spectra obtained in the experiment are shown in Fig. 2. Figure 2(a) shows a time-integrated x-ray emission spectrum from a $500 \times 500 \times 20$-μm^3 Cu target irradiated with an $E_L = 1000$ J, $\tau_p = 10$-ps pulse. Figure 2(b) shows an x-ray emission spectrum from a $75 \times 75 \times 5$-μm^3 Cu target irradiated with the same laser conditions.

The emission spectra show peaks at 8.05 and 8.91 keV, where the Cu plasma emits K_α and K_β inner-shell radiation. As hot electrons move through the target, the atomic electrons in the $1s$ shell of copper ions are ejected by electrons with energies 2 to 3 times the copper K-shell ionization potential ($\sim$ 20–25 keV). During deexcitation, the system relaxes to a lower-energy state, with $2p \rightarrow 1s$ and $3p \rightarrow 1s$ transitions generating K_α and K_β photons. The emission lines are fit to Gaussian line shapes with a full width at half maximum of 220 eV. The emission spectra contain the thermal He$_\alpha$ and Ly$_\alpha$ ionic-line emission that is generated from hot surface plasma on the laser-irradiated side of the target.

The main observation from these measurements is the suppressed K-photon yield from the reduced-mass target. The $75 \times 75 \times 5$-μm^3 Cu target generates no K_β radiation and has a dramatically suppressed K_α yield compared to the larger volume target. The suppressed K-photon yield

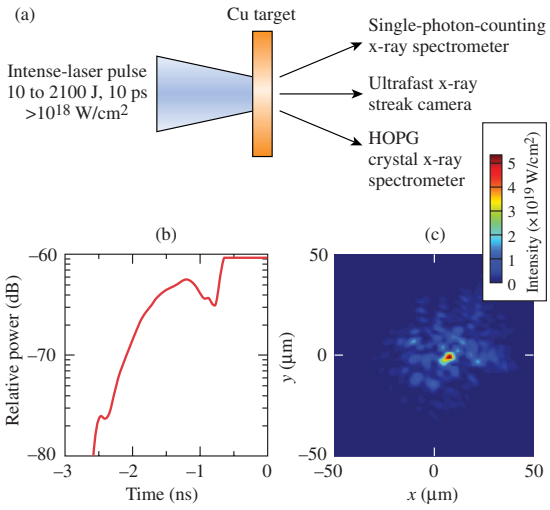

FIG. 1 (color online). (a) Experimental setup. (b) OMEGA EP optical-contrast measurement up to 0.5 ns before the main pulse ($E_L = 1000$ J, $\tau_p = 10$ ps). (c) OMEGA EP focal-spot image for an $E_L = 1000$ J, $\tau_p = 10$-ps pulse.

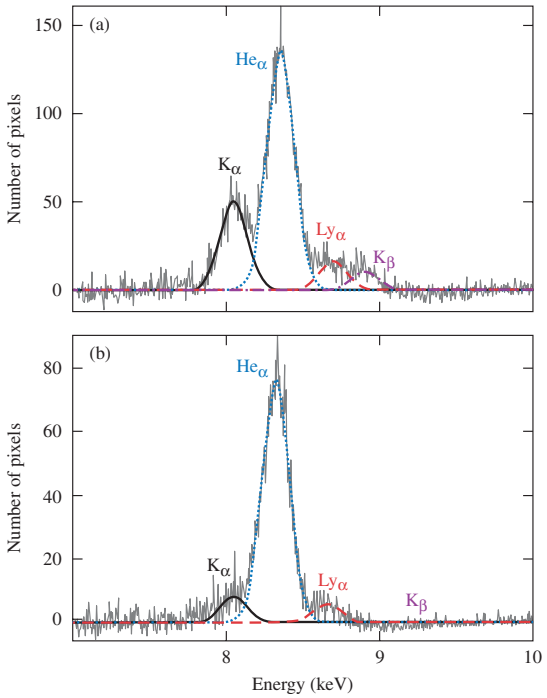

FIG. 2 (color online). Comparison of K-photon emission spectra from (a) $500 \times 500 \times 20$-μm and (b) $75 \times 75 \times 5$-μm^3 Cu targets irradiated with $E_L = 1000$-J, $\tau_p = 10$-ps laser pulses.

suggests higher-energy density conditions and high thermal-electron temperatures in the reduced-mass target. This is expected for these high-energy interaction conditions [14–16,29,30].

The method for calculating $\eta_{L\text{-}e}$ involves comparing K-photon emission from reduced-mass targets to target-heating calculations and was described previously in Ref. [15]. It relies on a significant fraction of the laser-generated hot electrons being trapped by the target potential that develops because of the charge separation that occurs between the hot escaping electrons and the relatively immobile ions [12]. This effect has been studied theoretically [15] and confirmed experimentally [14,16,29,30]. The collisional range of MeV electrons in cold, solid-density Cu is several hundred microns and is much greater than the target thickness used in the experiment. Hot electrons recirculate (reflux) throughout the target, efficiently transferring energy to the target material until they range out. Capacitance model calculations indicate that hot-electron refluxing efficiencies in these targets reach >90%, making K-photon spectroscopy measurements of the contained hot electrons highly representative of $\eta_{L\text{-}e}$.

Time-resolved x-ray emission measurements support the electron-refluxing interpretation for $\tau_p = 10$-ps pulses. Figure 3 shows the radiation time history for a $100 \times 100 \times 10$-μm^3 Cu target irradiated with an $E_L = 1000$-J, $\tau_p = 10$-ps pulse. The ultrafast x-ray streak camera was filtered with 25-μm-thick Be and 20-μm-thick Al foils [Fig. 3 (inset)].

An increase in radiation emission correlated with the laser-pulse duration, implying an increasing hot-electron number density within the target over this period. This occurs because hot electrons reflux, suggesting constant laser-energy coupling to hot electrons over the entire duration of the incident laser drive. After the laser pulse ends, a radiation afterglow persists for around 20 ps (FWHM) and is likely a combination of inner-shell radiation and thermal radiation, emitted in response to the electron-energy deposition within the target. Thermal radiation persists until the hot electrons thermalize and target decompression dominates.

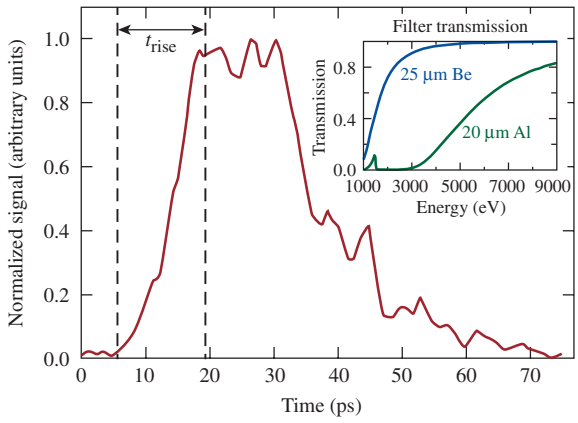

FIG. 3 (color online). Time-resolved x-ray emission from a $100 \times 100 \times 10$-μm^3 Cu target ($E_L = 1000$ J, $\tau_p = 10$ ps). The transmission functions for the x-ray streak camera filters are shown (inset).

The absolute K-photon yield generated during the recirculation phase is sensitive to the time-varying number density of hot electrons within the target and target heating. The target-charging process governs the number of hot electrons contained within the target, while target heating is caused mainly by electron-electron collisional energy deposition from the hot electrons. The ionization state of the target depends on collisions between bound and free conduction electrons. Once the thermal-electron temperature inside the target exceeds a few hundred electron volts, the Cu M shell is depleted by thermal ionization, suppressing the plasma's ability to generate K_β photons. Several hundreds of electron volts are required to deplete the Cu L shell. Time-integrated K-photon emission measurements quantify the target heating, making it possible for $\eta_{L\text{-}e}$ to be inferred by comparison to target-heating calculations, which are used to predict the ratio of K_β to K_α (K_β/K_α) for a given hot-electron conversion efficiency.

The data show that suppression of the K-photon yield is governed by target-energy density. Figure 4 shows the experimentally measured values for K_β/K_α from reduced-mass targets plotted as a function of the ratio of the laser energy to the target volume. The data obtained with 10-ps pulses (solid and open blue data points) are compared to previously published data with 1-ps pulses (black data points) [16]. The measured values for K_β/K_α are normalized to those measured from Cu foils when target heating is negligible ($K_\beta/K_\alpha \sim 0.14$).

A reduction in the K_β/K_α ratio is observed with increasing laser energy and decreasing target volume. At the lowest target-energy densities studied ($\sim 1.5 \times 10^3$ J/mm^3), laser-generated hot electrons interact with cold target material. When the target-energy density is increased to greater than 1×10^5 J/mm^3, target heating and thermal ionization suppress K_β/K_α. For target-energy densities of $\sim 5 \times 10^5$ J/mm^3, K_β/K_α is suppressed to $40 \pm 4\%$ of the cold-material value.

The experimental trend in K_β/K_α with $\tau_p = 10$-ps pulses is in excellent agreement with previous studies that were performed at significantly lower, joule-class laser energies and picosecond-pulse durations [16]. The same rate of change in K_β/K_α is observed with increasing energy density, independent of laser-pulse duration from $1 \leq \tau_p \leq 10$ ps. For the parameter space studied, variations in laser spot size, laser intensity, laser prepulse, and angle of incidence do not alter this observation. Scaled for laser energy and target mass, the results from these experiments suggest that the same fraction of laser energy is transferred into K-photon-generating hot electrons, independent of laser-pulse duration.

This interpretation is supported by two-dimensional, cylindrically symmetric target-heating calculations using

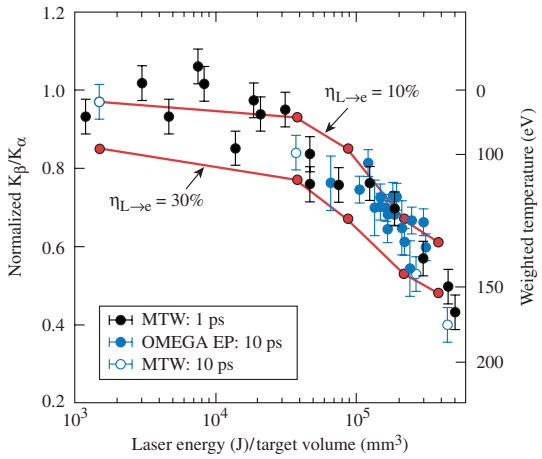

FIG. 4 (color online). Experimental K_β/K_α data normalized to the cold-material value (left axis) and inferred bulk-electron temperature (right axis) as a function of laser energy (J)/target volume (mm^3). Data are shown for 10-ps pulses from OMEGA EP (solid blue circles: $300 \leq E_L \leq 2100$ J, $500 \times 500 \times 20 \leq V \leq 600 \times 600 \times 50$ μm^3) and MTW (open blue circles: $E_L \leq 10$ J, $75 \times 75 \times 3 \leq V \leq 500 \times 500 \times 20$ μm^3). Data for 1-ps pulses (black circles) are reproduced from Ref. [16]. Target-heating calculations are shown for $\eta_{L\text{-}e} = 10\%$ and 30%.

the implicit-hybrid particle-in-cell code LSP [31]. Self-generated fields are included in the model and are calculated self-consistently. Target charging and heating in the calculations were produced by a hot-electron population that has an exponential energy distribution, with a temperature of up to several hundred keV, as defined by the ponderomotive scaling [20] and the range of experimental laser irradiation conditions. Spatial and temporal heating variations are accounted for when determining K-photon emission, with the emission probability calculated using the local temperature at the time of emission. The Thomas-Fermi equation-of-state model used is appropriate for the range of temperatures achieved in this experiment.

The calculated values for K_β/K_α as a function of increasing energy density are shown in Fig. 4. Calculations were performed assuming $\eta_{L\text{-}e} = 10\%$ and 30%. The target-heating model predicts suppression in K_β/K_α very similar to that observed in the experiment. The thermal-electron temperature inferred from the model for different target interactions is shown in Fig. 4 (right axis). This temperature represents a measure of the degree of target heating by hot-electron energy deposition and is weighted by the K-photon emission rate. Weighted thermal-electron temperatures approaching several hundred electron volts are achieved in the smallest-mass targets.

Strong reduction of K_β/K_α in the calculations supports the interpretation that in hot Cu-foil targets, thermal ionization causes K-photon suppression with hot-electron refluxing being the dominant energy transfer mechanism. An energy-coupling efficiency to hot electrons of $\eta_{L\text{-}e} = 20 \pm 10\%$ reproduces the majority of the experimental $\tau_p = 10$-ps data. This range of $\eta_{L\text{-}e}$ is in good agreement with previous $\tau_p = 1$-ps studies at similar laser intensities [15,16].

In summary, thin-foil targets have been heated with hot electrons that were generated by a $\tau_p = 10$-ps pulse at focused intensities of $I > 10^{18}$ W/cm^2. K-photon spectroscopy and target-heating calculations show an energy-coupling efficiency into hot electrons of $\eta_{L\text{-}e} \sim 20\%$ with laser powers from $1 \leq P_L \leq 210$ TW. These measurements are in excellent agreement with previous $\tau_p = 1$-ps data at similar laser intensities, demonstrating that the energy-conversion efficiency into hot electrons is independent of laser-pulse duration from $1 \leq \tau_p \leq 10$ ps. These results are important for the understanding of hot-electron generation in long-pulse, high-intensity laser-solid interactions, such as those found in fast-ignition and high-brightness x-ray-generation experiments.

This work was supported by the U.S. Department of Energy Office of Inertial Confinement Fusion under Cooperative Agreements No. DE-FC52-08NA28302 and No. DE-FC02-04ER54789, the University of Rochester, and the New York State Energy Research and Development Authority.

[1] M. I. K. Santala *et al.*, Phys. Rev. Lett. **84**, 1459 (2000).
[2] E. L. Clark *et al.*, Phys. Rev. Lett. **84**, 670 (2000).
[3] R. A. Snavely *et al.*, Phys. Rev. Lett. **85**, 2945 (2000).
[4] P. K. Patel *et al.*, Phys. Rev. Lett. **91**, 125004 (2003).
[5] B. A. Remington *et al.*, Science **284**, 1488 (1999).
[6] M. H. Key *et al.*, Phys. Plasmas **5**, 1966 (1998).
[7] M. Tabak *et al.*, Phys. Plasmas **1**, 1626 (1994).
[8] D. F. Price *et al.*, Phys. Rev. Lett. **75**, 252 (1995).
[9] H. Chen *et al.*, Phys. Rev. Lett. **70**, 3431 (1993).
[10] K. B. Wharton *et al.*, Phys. Rev. Lett. **81**, 822 (1998).
[11] K. Yasuike *et al.*, Rev. Sci. Instrum. **72**, 1236 (2001).
[12] S. P. Hatchett *et al.*, Phys. Plasmas **7**, 2076 (2000).
[13] F. N. Beg *et al.*, Phys. Plasmas **4**, 447 (1997).
[14] W. Theobald *et al.*, Phys. Plasmas **13**, 043102 (2006).
[15] J. Myatt *et al.*, Phys. Plasmas **14**, 056301 (2007).
[16] P. M. Nilson *et al.*, Phys. Rev. E **79**, 016406 (2009).
[17] L. J. Waxer *et al.*, Opt. Photonics News **16**, 30 (2005).
[18] F. Perez *et al.*, Phys. Rev. Lett. **104**, 085001 (2010).
[19] A. J. Kemp, Y. Sentoku, and M. Tabak, Phys. Rev. Lett. **101**, 075004 (2008).
[20] S. C. Wilks *et al.*, Phys. Rev. Lett. **69**, 1383 (1992).
[21] K. U. Akli *et al.*, Phys. Rev. Lett. **100**, 165002 (2008).
[22] V. Bagnoud *et al.*, Opt. Lett. **30**, 1843 (2005).
[23] V. Bagnoud *et al.*, Opt. Express **15**, 5504 (2007).
[24] J. Bromage *et al.*, Opt. Express **16**, 16 561 (2008).
[25] J. Delettrez *et al.*, Phys. Rev. A **36**, 3926 (1987).
[26] C. Stoeckl *et al.*, Rev. Sci. Instrum. **75**, 3705 (2004).
[27] A. Pak *et al.*, Rev. Sci. Instrum. **75**, 3747 (2004).
[28] C. Stoeckl *et al.*, Bull. Am. Phys. Soc. **52**, 67 (2007).
[29] S. D. Baton *et al.*, High Energy Density Phys. **3**, 358 (2007).
[30] G. Gregori *et al.*, Contrib. Plasma Phys. **45**, 284 (2005).
[31] D. R. Welch *et al.*, Phys. Plasmas **13**, 063105 (2006).